

Article

u -Channel Color Transparency Observables

Garth M. Huber ¹ , Wenliang B. Li ^{2,3,*} , Wim Cosyn ^{4,5}  and Bernard Pire ⁶ ¹ Department of Physics, University of Regina, Regina, SK S4S 0A2, Canada; huberg@uregina.ca² Center for Frontiers in Nuclear Science, Stony Brook University, Stony Brook, NY 11794, USA³ Department of Physics and Astronomy, Stony Brook University, Stony Brook, NY 11794, USA⁴ Department of Physics, Florida International University, Miami, FL 3199, USA; wcosyn@fiu.edu⁵ Department of Physics and Astronomy, Ghent University, 9000 Gent, Belgium⁶ The Center for Theoretical Physics (CPHT), CNRS, École Polytechnique, Institut Polytechnique de Paris, 91128 Palaiseau, France; bernard.pire@polytechnique.edu

* Correspondence: billlee@jlab.org

Abstract: The paper proposes to study the onset of color transparency in hard exclusive reactions in the backward regime. Guided by the encouraging Jefferson Laboratory (JLab) results on backward π and ω electroproduction data at moderate virtuality Q^2 , which may be interpreted as the signal of an early scaling regime, where the scattering amplitude factorizes in a hard coefficient function convoluted with nucleon to meson transition distribution amplitudes, the study shows that investigations of these channels on nuclear targets opens a new opportunity to test the appearance of nuclear color transparency for a fast-moving nucleon.

Keywords: color transparency; u -channel meson production; collinear factorization

1. Introduction

Although a fundamental prediction of quantum chromodynamics (QCD) [1,2], the phenomenon of color transparency (CT) has been, for many decades, a domain of controversial interpretations of experimental data; for a review, see, e.g., [3]. Together with scaling laws and polarization tests, the increase in nuclear transparency (NT) ratio with the relevant hard scale (denoted as Q^2) is believed to constitute an important signal of the onset of a collinear QCD factorization regime where hadrons transverse sizes shrink proportionally to $1/Q$, thus drastically diminishing final-state interaction cross-sections.

Near forward exclusive photon or meson electroproduction processes have been the subject of intense theoretical and experimental studies [4,5]. Most of the available data are now interpreted in terms of a collinear QCD factorized amplitude, where generalized parton distributions (GPDs) are the relevant hadronic matrix elements. The study of nuclear transparency for meson electroproduction [6,7] indeed revealed a growth of the NT ratio indicative of an early on-set of the scaling regime. This may, however, look contradictory to the non-dominance of the leading twist pion production amplitude revealed by the small value of the virtual photon's longitudinal-to-transverse structure function ratio, σ_L/σ_T , for this reaction [8,9]. Alternative models have been proposed [10] to explain this fact.

Exclusive electroproduction processes in the complementary near backward region, where $-u = -(p_M - p_N)^2 \ll Q^2$ (see Figure 1 for definitions), is near its minimal value [11], should also be described at large Q^2 in a collinear QCD factorization scheme [12–14], where nucleon to meson transition distribution amplitudes (TDAs) replace the GPDs as the relevant hadronic matrix elements [15]. Indeed, the first experimental studies [16–18] of this new domain at rather moderate values of Q^2 point toward an early onset of the scaling regime.



Citation: Huber, G.M.; Li, W.B.; Cosyn, W.; Pire, B. u -Channel Color Transparency Observables. *Physics* **2022**, *4*, 451–461. <https://doi.org/10.3390/physics4020030>

Received: 9 February 2022

Accepted: 1 April 2022

Published: 22 April 2022

Publisher's Note: MDPI stays neutral with regard to jurisdictional claims in published maps and institutional affiliations.



Copyright: © 2022 by the authors. Licensee MDPI, Basel, Switzerland. This article is an open access article distributed under the terms and conditions of the Creative Commons Attribution (CC BY) license (<https://creativecommons.org/licenses/by/4.0/>).

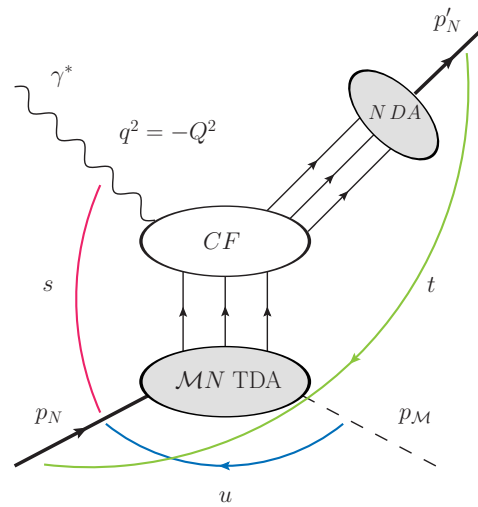


Figure 1. Kinematical quantities and the collinear factorization mechanism for $\gamma^*N \rightarrow NM$ in the near-backward kinematical regime (large virtuality Q^2 , invariant mass W ; fixed Bjorken x (or x_B); $|u| \sim 0$). q, p_N, p_M and p'_N are the four momenta of the virtual photon probe, initial state nucleon target, final state proton, and final state meson. The lower blob, denoted MN TDA, depicts the nucleon-to-meson M transition distribution amplitude; the N DA blob depicts the nucleon distribution amplitude; CF denotes the hard subprocess amplitude (coefficient function). Here, s is the center-of-mass energy squared, and t and u denote the four momentum differences squared (Mandelstam variables). These are defined as $s = W^2 = (q + p_N)^2, t = (p'_N - p_N)^2, u = (p_M - p_N)^2$.

2. The Proposed Measurement

2.1. Previous Backward-Angle Data from Jefferson Laboratory (JLab)

The first data providing qualitative support for the TDA picture are from the JLab 6 GeV physics program [16–18].

Hard exclusive π^+ production ($ep \rightarrow e'n\pi^+$) from a polarized electron beam interacting with an unpolarized hydrogen target was studied with the CLAS detector in the backward angle kinematic regime by Park et al. [16]. Figure 2 shows the Q^2 -dependence of $\sigma_U = \sigma_T + \varepsilon\sigma_L$, interference contributions σ_{LT} and σ_{TT} , obtained at the average kinematics of invariant mass $W = 2.2$ GeV and $-u = 0.5$ GeV² (see Figure 1). ε describes the ratio of the fluxes of longitudinal and transverse virtual photons. All three cross-sections have a strong Q^2 -dependence. The TDA formalism predicts that the transverse amplitude dominates at large Q^2 . With only this set of data at a fixed beam energy, the CLAS detector cannot experimentally separate σ_T and σ_L . After examining the angular dependence of σ_U , the results show σ_{TT} and σ_{LT} roughly equal in magnitude and with a similar Q^2 -dependence. Their significant sizes (about 50% of σ_U) imply an important contribution of the transverse amplitude in the cross-section. Furthermore, above $Q^2 = 2.5$ GeV², the trend of σ_U is qualitatively consistent with the TDA calculation, yielding the characteristic $1/Q^8$ dependence expected when the backward collinear factorization scheme is approached.

The beam spin asymmetry moment, $A_{LU}^{\sin\phi}$, with ϕ being the azimuthal angle from the scattering plane, was also extracted using the CLAS detector [18]. $A_{LU}^{\sin\phi}$ is proportional to the polarized structure function $\sigma_{LT'}$,

$$A_{LU}^{\sin\phi} = \frac{\sqrt{2\varepsilon(1-\varepsilon)} \sigma_{LT'}}{\sigma_T + \varepsilon\sigma_L}, \tag{1}$$

where the structure functions σ_L and σ_T correspond to longitudinally and transversely polarized virtual photons. Due to the large acceptance of CLAS, it was possible to map out the full kinematic region in $-t$ (defined in Figure 1 caption) from very forward kinematics ($-t/Q^2 \ll 1$) where a description based on Generalized Parton Distributions (GPD) can

be applied, up to very backward kinematics ($-u/Q^2 \ll 1$, $-t$ large), where a TDA-based description is expected to be valid. The results in Figure 3 indicate a transition from positive $A_{LU}^{\sin\phi}$ in the forward regime to rather small negative values in the backward regime, with a Q^2 dependence qualitatively consistent with the TDA picture. The sign change between the forward and backward kinematic regimes is independent of Q^2 and x_B within the kinematics accessible with CLAS.

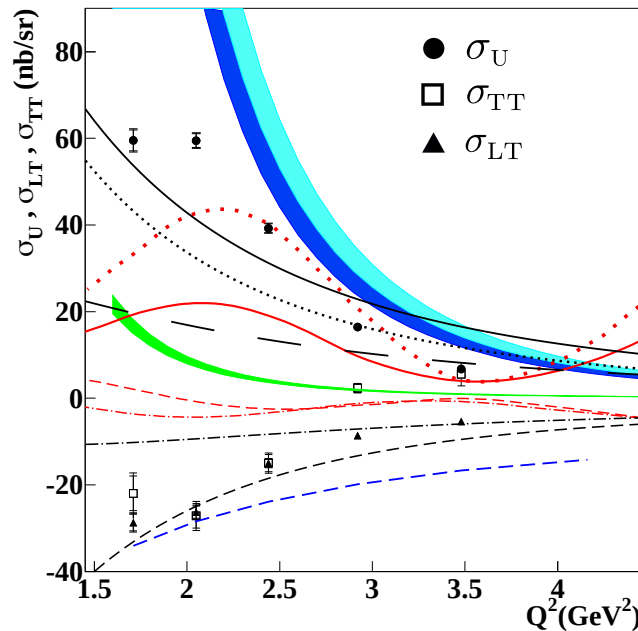


Figure 2. The structure functions, $\sigma_U = \sigma_T + \varepsilon\sigma_L$ (solid dot), σ_{TT} (square), and σ_{LT} (triangle), as a function of Q^2 . ε describes the ratio between longitudinally and transversely polarized virtual photons. The inner error bars are statistical and the outer error bars are the combined systematic and statistical uncertainties in quadrature. The bands refer to model calculations of σ_U in the TDA description, green band: Braun-Lenz-Wittmann next-to-next-to-leading-order (BLW NNLO), dark blue band: Chernyak-Ogloblin-Zhitnitsky (COZ), and light blue band: King-Sachrajda (KS) (see [16] and Refs. therein for the meaning of these models). The lower blue short-dashed line represents an educated guess to fit the higher twist cross-sections σ_{LT} and σ_{TT} in the TDA picture. The red curves are the “Regge” predictions (by JML18) of [19,20] for solid: σ_U , dashed curve: σ_{LT} , dot-dashed: σ_{TT} . An updated σ_U calculation from JML18 model [21] are shown in the red dotted curve. Regge calculations which consider parton contributions (see Ref. [11]) to $\sigma_U, \sigma_T, \sigma_L, \sigma_{TT}$ and σ_{LT} are shown in black solid, black dotted, black long-dashed, black dot-dashed, and black short-dashed, respectively. This plot was recreated from the data and model predictions published in Refs. [11,16].

Backward-angle exclusive ω electroproduction ($ep \rightarrow e'p\omega$) was studied in Hall C by Li et al. [17]. The scattered electron and forward-going proton were detected in the High Momentum Spectrometer (HMS) and Short Orbit Spectrometer (SOS), and the low-momentum rearward-going ω was reconstructed using the missing mass reconstruction technique. Since this method does not require the detection of the produced meson, it allows the analysis to extend the experimental kinematics coverage to a region that is inaccessible through the standard direct detection method. The extracted σ_L and σ_T as a function of $-u$ at $Q^2 = 1.6$ and 2.45 GeV^2 are shown in Figure 4. The two sets of TDA predictions [22] for σ_T each assume different nucleon DAs [23,24] as input. From the general trend, the TDA model offers a good description of the falling σ_T as a function of $-u$ at both Q^2 settings, similar to the backward-angle π^+ data from [16]. Together, the datasets are suggestive of early TDA scaling. The behavior of σ_L differs greatly at the two Q^2 settings. At $Q^2 = 1.6$ GeV^2 , σ_L falls almost exponentially as a function of $-u$; at $Q^2 = 2.45$ GeV^2 , σ_L is constant near zero (within one standard deviation). Note that the TDA model predicts

a small-higher twist- σ_L contribution, which falls faster with Q^2 than the leading twist σ_T contribution.

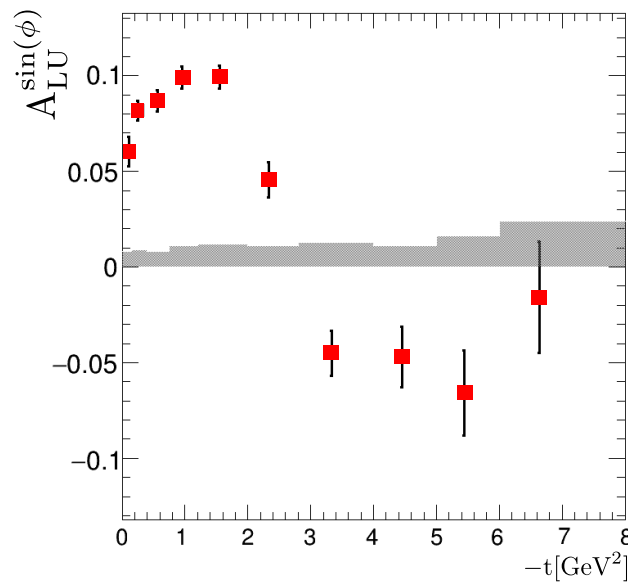


Figure 3. Beam-spin asymmetry moment, $A_{LU}^{\sin\phi}$ (Equation (1)), as a function of $-t$ measured with CLAS detector at $W > 2$ GeV, $Q^2 > 1$ GeV². The maximal accessible value of $-t$ is ≈ 8.8 GeV². The shaded area represents the systematic uncertainty. This plot was recreated from the data and model predictions published in Ref. [18].

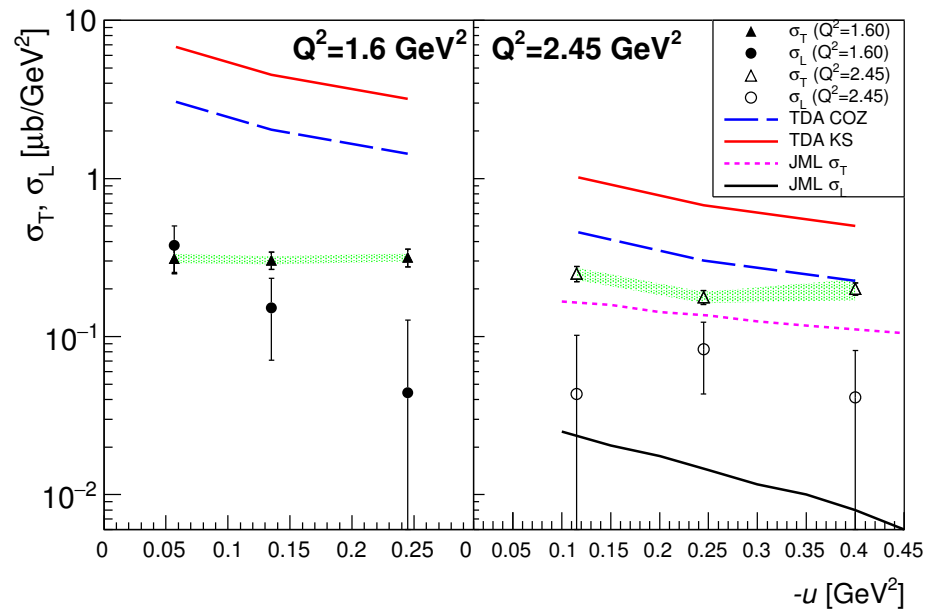


Figure 4. σ_T (triangles), σ_L (squares) as a function of $-u$, at $Q^2 = 1.6$ GeV² (left), 2.45 GeV² (right). For the lowest $-u$ bin, $u' = u - u_{\min} \approx 0$. TDA predictions for σ_T : COZ (blue dashed lines), KS (red solid lines). The predictions were calculated at the specific $\overline{Q^2}$, \overline{W} values of each u bin (overline represents the nominal value), and the predictions at three u bins joined by straight lines for visualization purpose. Green bands indicate correlated systematic uncertainties for σ_T , the uncertainties for σ_L are similar. This plot was recreated from the data and model predictions published in Ref. [17].

2.2. Jefferson Lab Proposal E12-20-007

The first dedicated experiment for exclusive π^0 production in backward kinematics ($ep \rightarrow e'p\pi^0$), was proposed by Li et al. in [25]. Here, the produced π^0 is emitted 180 degrees opposite to the virtual-photon momentum (at large momentum transfer), and is reconstructed via the missing mass technique, just as in [17]. This study aims to apply the Rosenbluth separation technique to provide model-independent L/T-separated differential cross-sections at the never explored u -channel kinematics region near ($-t = -t_{\max}$, $-u = -u_{\min}$).

The kinematic coverage of the experiment is shown in Figure 5. The L/T-separated cross-sections are planned at $Q^2 = 2.0, 3.0, 4.0,$ and 5.0 GeV^2 . These measurements will provide the $-u$ dependence for σ_L and σ_T at nearly constant Q^2 and W , in addition to the behavior of σ_L/σ_T ratio as function of Q^2 . The $Q^2 = 6.25 \text{ GeV}^2$ setting is chosen to test the Q^2 scaling nature of the unseparated cross-section, but only one ϵ setting is available due to limitations on the accessible spectrometer angles. These measurements are intended to provide a direct test of two predictions from the TDA model [26]: $\sigma_T \propto 1/Q^8$ and $\sigma_T \gg \sigma_L$ in u -channel kinematics. The magnitude and u -dependence of the separated cross-sections also provide direct connections to the re-scattering Regge picture [21]. The extracted interaction radius (from u -dependence) at different Q^2 can be used to study the soft-hard transition in the u -channel kinematics.

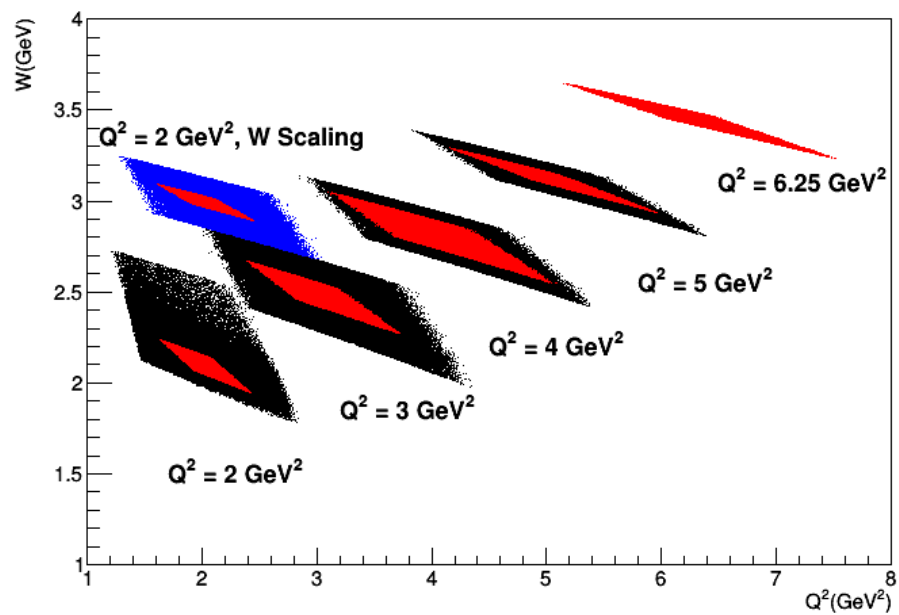


Figure 5. W vs. Q^2 diamonds for the $Q^2 = 2.0, 3.0, 4.0, 5.0,$ and 6.25 GeV^2 settings of the Jefferson Laboratory proposal E12-20-007. The black diamonds are for the higher ϵ settings and the red diamonds are for the lower ϵ settings. The diamonds for the W scaling setting are shown separately (in blue and red). Note that there is only one ϵ setting for $Q^2 = 6.25 \text{ GeV}^2$. The overlap between the black and red diamond is critical for the L/T separation at each setting. The boundary of the low ϵ (red) data coverage will become a cut for the high ϵ data. See text for details.

Relevant to this discussion is the definition of skewness. For forward-angle kinematics, in the regime where the handbag mechanism and GPD description may apply, the skewness is defined in the usual manner,

$$\zeta_t = \frac{p_1^+ - p_2^+}{p_1^+ + p_2^+}, \tag{2}$$

where p_1^+, p_2^+ refer to the light-cone plus components of the initial and final proton momenta [4]. The subscript t has been added to indicate that this skewness definition is typically used for forward-angle kinematics, where $-t \rightarrow -t_{\min}$. In this regime, ζ_t is related

to x_B , and is approximated by $\zeta_t = x/(2-x)$, up to corrections of order $t/Q^2 < 1$ [4]. This relation is an accurate estimate of ζ_t to the few percent level for forward-angle electroproduction. In backward-angle kinematics, where $-t \rightarrow -t_{\max}$ and $-u \rightarrow -u_{\min}$, the skewness is defined with respect to u -channel momentum transfer in the TDA formalism [15],

$$\zeta_u = \frac{p_1^+ - p_\pi^+}{p_1^+ + p_\pi^+}. \tag{3}$$

Figure 6 shows the forward ζ_t and backward ζ_u skewness coverage of the approved measurements. The “soft–hard transition” in u -channel meson production is an interesting and unexplored subject. The acquisition of these data will be an important step forward in validating the existence of a backward factorization scheme of the nucleon structure function and establishing its applicable kinematic range.

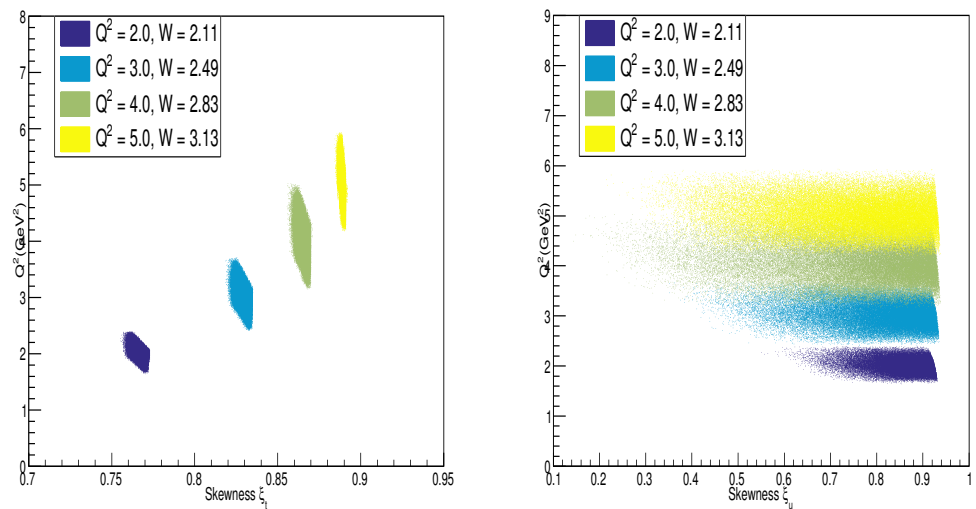


Figure 6. Forward skewness ζ_t (**left**) and backward skewness ζ_u (**right**) coverage of the planned E12-20-007 measurements for $Q^2 = 2.0$ to 5.5 GeV^2 (see text for definitions). Clearly the experiment probes a wide kinematic range, which will be helpful for distinguishing the roles of the TDA and Regge reaction mechanisms in the soft–hard transition range.

2.3. Nuclear Targets

Since the JLab 6 GeV backward-angle data are qualitatively consistent with early factorization in backward kinematics, backward-angle meson production events with a high momentum forward proton may provide an alternate means of probing color transparency.

Exclusive π^0 production is considered as an example reaction, based on the kinematics of E12-20-007, but the technique is in principle extendable also to vector meson production. In this case, the scattered electron would be detected in the HMS and the high-momentum forward-going proton detected in the Super High Momentum Spectrometer (SHMS) of Hall C, with the meson reconstructed via the missing mass technique. Table 1 shows an example of kinematics (at JLab 12 GeV) for the described measurement. A comprehensive experiment should cover a range of nuclear targets, such as ^1H , ^{12}C , ^{27}Al , ^{63}Cu , and ^{197}Au , aiming to get broadly similar statistical uncertainties for all targets.

Based on the simulations performed for E12-20-007 [25], and the experience of the earlier π^+ Hall C nuclear transparency experiment [6], the main physics background within the spectrometer acceptance is expected to come from multi-pion production. The lower limit for the two-pion production phase-space is estimated to be $m_{\text{missing}}^2 \sim 0.06 \text{ GeV}^2$ for a ^1H target. Due to Fermi smearing, the reconstruction resolution will be somewhat worse for the data from heavier nuclei, but this effect can be included in the simulations used to optimize the experimental cuts to be used for each nuclear target. In [6], the estimated multi-pion background contamination was $< 0.4\%$, so it is reasonable to expect this contamination

to be no larger than a few percent here. The contamination of higher mass mesons (such as η and ρ) should be negligible. The remaining physics background would come from virtual Compton scattering (VCS). Although the missing mass reconstruction resolution will not allow the π^0 and VCS channels to be separated, this contamination is also expected to be $<1\%$. Thus, the Hall C standard equipment should allow high-quality u -channel data to be acquired from nuclear targets, and allow nuclear transparency to be studied in backward exclusive π^0 electroproduction.

Table 1. Possible kinematics for a backward angle color transparency experiment in Hall C of Jefferson Laboratory. The approximate momentum and the angle of the detected scattered electron and proton, and the undetected π^0 are shown along with the expected t, u ranges covered by the data. See text for details.

$A(e, e'p)\pi^0$ Kinematics for $E_{\text{beam}} = 10.6 \text{ GeV}, W = 2 \text{ GeV}$					
$Q^2 \text{ (GeV}^2\text{)}$	$e' \text{ (GeV/c, deg)}$	$p \text{ (GeV/c, deg)}$	$\pi^0 \text{ (GeV/c, deg)}$	$t \text{ (GeV}^2\text{)}$	$u \text{ (GeV}^2\text{)}$
3	7.3, 11.3°	3.9–3.6, 23°–30°	0.2–0.5, 202°–95°	–5.7 to –5.2	+0.5 to –0.1
6	5.7, 18.1°	5.6–5.2, 19°–24°	0.1–0.5, 196°–79°	–8.8 to –8.2	+0.6 to 0.0
10	3.6, 29.7°	7.7–7.3, 13°–16°	0.0–0.5, 193°–61°	–12.8 to –12.1	+0.6 to –0.1

2.4. Electron-Ion Collider (EIC) Perspective

Despite the difference in the configuration compared to the JLab 12 GeV fixed target experiment, the future EIC [27–29] can be used to probe u -channel CT via meson electroproduction: $e + p \rightarrow e' + p' + \pi^0$ and $e + A(Z) \rightarrow e' + p' + A'(Z - 1) + \pi^0$, where Z is the atomic number of the ion A beam. To directly extend the kinematics coverage (in Q^2) of the JLab measurement, the preferred beam scattering configuration requires a 5 GeV electron beam to collide with a 100 GeV per nucleon ion beam. It is important to note that EIC will offer a variety of ion beams, see details in Ref. [30]. The proposed measurement utilizes the electron and hadron end-caps, and integrated instrumentation in the far forward region (downstream of the outgoing ion beamline). The detection scenario is the following: the scattered electron will be captured by the electron end-cap; the induced virtual photon interacts with a nucleon within the nucleus, then the interacted nucleon transitions into a final state π^0 through TDA (in u -channel kinematics, see Figure 1); the fast proton (knocked out of the nucleus) will be picked up by the hadron end-cap and create a “start” in the timing window; the π^0 moves out of the nucleus and decays into two photons, thus projecting a one or two-photon signal in the far forward B0 or Zero Degree Calorimeter. In the case of eA scattering, the $A(Z)$ loses a proton due to the interaction and becomes $A'(Z - 1)$, and can be captured by the Roman Pot detector due to the loss of total momentum and magnetic field steering. The feasibility of such a measurement is currently being studied by the EIC Comprehensive Chromodynamics Experiment (ECCE) consortium.

Here, it is important to point out that the color transparency study has been proposed at the EIC through $e + p$ and $e + A$ scatterings, and photoproduction of mesons [29,31]. These CT studies are based on the validity of collinear factorization theme in the small $-t$ kinematics, and should be distinguished from the u -channel meson electroproduction observable proposed in this paper. In the former case, a final state meson will be produced by the $e + p$ and $e + A$ interactions, and will be detected by the central barrel of the EIC; in the latter case, the interacted ion beam and the newly produced meson will both enter the far forward region, as described above.

3. A Model Estimate of Nuclear Transparency

For the $^{12}\text{C}, ^{27}\text{Al}, ^{63}\text{Cu}$, and ^{197}Au nuclei, estimates for the $A(e, e'p)\pi A - 1$ nuclear transparency in the backward regime kinematics of Table 1 available in JLab Hall C is given here. These estimates are obtained using the relativistic multiple scattering Glauber approximation (RMSGa). The RMSGa is a flexible framework that treats kinematics and dynamics (nuclear wave functions, final-state interactions (FSI)) relativistically and has

been applied to a variety of hadron-, electron-, and neutrino-induced nuclear reactions; see [32–35] and references therein. The NT ratio is calculated as

$$T = \frac{\sigma^{\text{RMSGA}}}{\sigma^{\text{PWIA}}}, \tag{4}$$

where, in the calculation of the plane wave impulse approximation (PWIA) denominator, FSI are turned off and nominator and denominator are integrated over the experimentally accessible phase space. The cross-section is calculated in a factorized form [34]:

$$\frac{d\sigma^{eA}}{dE_{e'}d\Omega_{e'}dud\phi_N ds_2} = \int d\Omega_{\pi}^* \frac{m_{A-1}}{4s_2} \sqrt{\frac{\lambda(s_2, m_{\pi}, m_{A-1})\lambda(s_{\gamma N}, m_N, -Q^2)}{\lambda(s_{\gamma A}, m_A, -Q^2)}} \times \rho_D(\mathbf{p}_i) \frac{d\sigma^{eN}}{dE_{e'}d\Omega_{e'}dud\phi_{\pi}}, \tag{5}$$

with integration over the solid angle of the (undetected) pion in the $(\pi, A - 1)$ center-of-mass system. In the above equation, $u = (q - p_N)^2$, and the function,

$$\lambda(s, m_1, m_2) = [s - (m_1 - m_2)^2][s - (m_1 + m_2)^2] \tag{6}$$

was used. Here, the invariant masses squared $s = (p_{\pi} + p_{A-1})^2, s_{\gamma N} = (q + p_i)^2, s_{\gamma A} = (q + p_A)^2$, are introduced where p_N, p_{π} and p_{A-1} are the four-momenta of the final state proton, pion, and remnant $A - 1$ nucleus, and

$$p_i = p_N + p_{\pi} - q \tag{7}$$

is the four-momentum of the initial struck nucleon. The nuclear initial state enters in the distorted momentum distribution,

$$\rho_D(\mathbf{p}_i) \equiv \sum_{m_s, \alpha_1} |\bar{u}(\mathbf{p}_i, m_s)\phi_{\alpha_1}^D(\mathbf{p}_i)|^2, \tag{8}$$

where the sum over α_1 runs over the quantum numbers of the occupied mean-field single particle levels of the initial nucleus A . Here, m_s is the spin quantum number of the free spinor. The Dirac spinor wave functions $\phi_{\alpha_1}^D$ include the effects of the FSI between the detected nucleon and the remnant $A - 1$ nucleus:

$$\phi_{\alpha_1}^D(\mathbf{p}) = \frac{1}{(2\pi)^{3/2}} \int d^3r e^{-i\mathbf{p}\cdot\mathbf{r}} \phi_{\alpha_1}(\mathbf{r})\mathcal{F}^{\text{FSI}}(\mathbf{r}). \tag{9}$$

The FSI entering in $\mathcal{F}^{\text{FSI}}(\mathbf{r})$ are parametrized using nucleon–nucleon scattering data; see [34] for details. In the PWIA calculation, $\mathcal{F}^{\text{FSI}}(\mathbf{r}) \rightarrow 1$ is set. The CT effects are implemented through the color diffusion model [36,37], using $\Delta M^2 = 1.1 \text{ GeV}^2$ in the nucleon coherence length $l_h = 2p_N/\Delta M^2$. The last ingredient of Equation (5) is the pion production cross-section on the nucleon, σ^{eN} , which was parameterized in the backward kinematics by interpolating the estimates provided in Ref. [25] (see Figure 19 and Appendix A therein), based on the model of Ref. [26].

Figure 7 shows the results of our calculations, where the central values from Table 1 are taken for the final state electron and proton kinematics. The transparency values lie in the expected range known from $A(e, e'p)$ calculations. These estimates show that the proposed experiment should be able to distinguish color transparency effects. Note that these predictions can be further improved with a detailed Monte Carlo simulation study and can be extended to EIC kinematics.

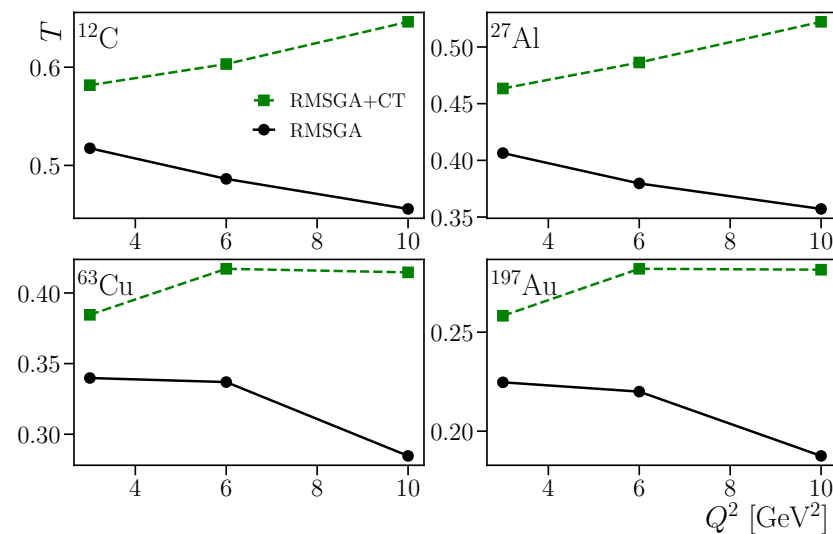


Figure 7. RMSGA nuclear transparency calculations for ¹²C, ²⁷Al, ⁶³Cu, and ¹⁹⁷Au as a function of Q^2 . Full curves are regular Glauber calculations, the dashed curves include the color transparency in the quantum diffusion model. See text for details.

4. Summary

The available data on nuclear transparency lead to the conclusion that the phenomenon of color transparency needs to be further explored. This is particularly important for the nucleon case. The historical measurement [38] of the large angle proton-proton (pp) elastic and quasi-elastic ($p, 2p$) scattering have led to many debates and interpretations [36,39–41].

The ($e, e'p$) measurements are a natural place to look for proton color transparency (CT). The recent data on the ($e, e'p$) reaction [42] demonstrated the absence of any positive signal for the manifestation of color transparency in this simple reaction up to $Q^2 = 14$ GeV², reinforcing doubts on the leading twist dominance of the nucleon form factors at experimentally available energy (especially at Jefferson Laboratory (JLab) experiment at 12 GeV). With transparency measurements available so far in a limited set of reactions and kinematics, it is too early to tell what drives the absence of the onset of CT in the proton case, while for forward meson production the onset has been observed. Planned measurements at JLab will extend the known meson production processes to the maximum Q^2 values available using the 12 GeV beam at JLab. In this paper a complement to this existing color transparency program is described which expands the study to an unexplored territory of u -channel kinematics ($t \rightarrow t_{\max}$).

For the first time, backward meson electroproduction on nuclei is linked to CT studies via the collinear QCD factorization framework. It is important to point out that the observation of CT is based on the assumption that a short distance process dominates the amplitude at reachable energies, hence the transition distribution amplitude (TDA) predictions are validated by the experimental data. Observation of CT will help to settle the controversy on the early scaling of exclusive reactions involving nucleons, by answering the question: does the exclusive meson electroproduction experiment witness the dominance of a small nucleon configuration in the backward kinematics where the nucleon has a large energy?

In a similar line of thought to this proposal, one may study nuclear transparency in various experiments (see [43]), where TDAs appear as the collinear factorized hadronic matrix element, while a hard scattering process should be accompanied by the appearance of color transparency. This is the case for timelike Compton scattering with a quasi-real photon beam [44], but also in the antiproton nucleus electromagnetic processes at PANDA experiment [45] and the π -nucleus program at J-PARC [46]. In these three cases, color transparency should act as a decrease in the initial (rather than final) state interactions.

Once the proposed measurement is completed, a broader discussion within the community is necessary to determine the implication and the global significance of the observed experimental facts, i.e., validation of the TDA formalism, presence or absence of an onset of CT.

Author Contributions: G.M.H., W.B.L., W.C. and B.P. contributed equally to this work. All authors have read and agreed to the published version of the manuscript.

Funding: The work of W.C. is partially supported by the National Science Foundation under Award No. 2111442. The work of G.M.H. is supported by the Natural Sciences and Engineering Research Council of Canada (NSERC), SAPIN-2021-00026.

Data Availability Statement: Not applicable.

Acknowledgments: We acknowledge numerous fruitful discussions with P. Jain, J.P. Ralston, K. Semenov-Tian-Shansky, and L. Szymanowski.

Conflicts of Interest: The authors declare no conflict of interest.

References

1. Mueller, A.H. Topics in high-energy perturbative QCD including interactions with nuclear matter. In Proceedings of the 17th Rencontres de Moriond on Elementary Particle Physics: I. Electroweak Interactions and Grand Unified Theories, Les Arcs, France, 14–20 March 1982; pp. 13–43.
2. Brodsky, S.J. Testing quantum chromodynamics. In Proceedings of the XIII International Symposium on Multiparticle Dynamics, Volendam, The Netherlands, 6–11 June 1982; Kittel, W.E., Metzger, W.J., Stergiou, A., Eds.; World Scientific: Singapore, 1982; pp. 963–1002.
3. Jain, P.; Pire, B.; Ralston, J.P. Quantum color transparency and nuclear filtering. *Phys. Rep.* **1996**, *271*, 67–179. [[CrossRef](#)]
4. Diehl, M. Generalized parton distributions. *Phys. Rept.* **2003**, *388*, 41–277. [[CrossRef](#)]
5. Kumericki, K.; Liuti, S.; Moutarde, H. GPD phenomenology and DVCS fitting: Entering the high-precision era. *Eur. Phys. J. A* **2016**, *52*, 157. [[CrossRef](#)]
6. Clasie, B.; Qian, X.; Arrington, J.; Asaturyan, R.; Benmokhtar, F.; Boeglin, W.; Bosted, P.; Bruell, A.; Christy, M.E.; Chudakov, E.; et al. Measurement of nuclear transparency for the $A(e, e'\pi^+)$ reaction. *Phys. Rev. Lett.* **2007**, *99*, 242502.
7. El Fassi, L.; Zana, L.; Hafidi, K.; Holtrop, M.; Mustapha, B.; Brooks, W.; Hakobyan, H.; Zheng, X.; Adhikari, K.; Adikaram, D.; et al. Evidence for the onset of color transparency in ρ^0 electroproduction off nuclei. *Phys. Lett. B* **2012**, *712*, 326–330.
8. Defurne, M.; Mazouz, M.; Ahmed, Z.; AlBataineh, H.; Allada, K.; Aniol, K.A.; Bellini, V.; Benali, M.; Boeglin, W.; Bertin, P.; et al. Rosenbluth separation of the π^0 electroproduction cross section. *Phys. Rev. Lett.* **2016**, *117*, 262001.
9. Dlamini, M.; Karki, B.; Ali, S.F.; Lin, P.-J.; Georges, F.; Ko, H.-S.; Israel, N.; Rashad, M.N.H.; Stefanko, A.; Adikaram, D.; et al. Deep exclusive electroproduction of π^0 at high Q^2 in the quark valence regime. *Phys. Rev. Lett.* **2021**, *127*, 152301.
10. Kaskulov, M.M.; Mosel, U. Deep exclusive charged π electroproduction above the resonance region. *Phys. Rev. C* **2010**, *81*, 045202. [[CrossRef](#)]
11. Ayerbe Gayoso, C.; Bibrzycki, L.; Diehl, S.; Heppelmann, S.; Higinbotham, D.W.; Huber, G.M.; Kay, S.J.D.; Klein, S.R.; Laget, J.M.; Li, W.B.; et al. Progress and opportunities in backward angle (u -channel) physics. *Eur. Phys. J. A* **2021**, *57*, 342.
12. Frankfurt, L.; Pobylitsa, P.; Polyakov, M.V.; Strikman, M. Hard exclusive pseudoscalar meson electroproduction and spin structure of a nucleon. *Phys. Rev. D* **1999**, *60*, 014010. [[CrossRef](#)]
13. Pire, B.; Szymanowski, L. Hadron annihilation into two photons and backward VCS in the scaling regime of QCD. *Phys. Rev. D* **2005**, *71*, 111501. [[CrossRef](#)]
14. Pire, B.; Szymanowski, L. QCD analysis of $\bar{p}N \rightarrow \gamma^* \pi$ in the scaling limit. *Phys. Lett. B* **2005**, *622*, 83–92. [[CrossRef](#)]
15. Pire, B.; Semenov-Tian-Shansky, K.; Szymanowski, L. Transition distribution amplitudes and hard exclusive reactions with baryon number transfer. *Phys. Rept.* **2021**, *940*, 2185.
16. Park, K.; Guidal, M.; Gothe, R.; Pire, B.; Semenov-Tian-Shansky, K.; Laget, J.-M.; Adhikari, K.; Adhikari, S.; Akbar, Z.; Avakian, H.; et al. Hard exclusive pion electroproduction at backward angles with CLAS. *Phys. Lett.* **2018**, *B780*, 340–345. [[CrossRef](#)]
17. Li, W.B.; Huber, G.M.; Blok, H.P.; Gaskell, D.; Horn, T.; Semenov-Tian-Shansky, K.; Pire, B.; Szymanowski, L.; Laget, J.-M.; Aniol, K.; et al. Unique access to u -channel physics: Exclusive backward-angle omega meson electroproduction. *Phys. Rev. Lett.* **2019**, *123*, 182501. [[CrossRef](#)] [[PubMed](#)]
18. Diehl, S.; Joo, K.; Kim, A.; Avakian, H.; Kroll, P.; Park, K.; Riser, D.; Semenov-Tian-Shansky, K.; Tezgin, K.; Adhikari, K.P.; et al. Extraction of beam-spin asymmetries from the hard exclusive π^+ channel off protons in a wide range of kinematics. *Phys. Rev. Lett.* **2020**, *125*, 182001. [[CrossRef](#)]
19. Guidal, M.; Laget, J.M.; Vanderhaeghen, M. Pseudoscalar meson photoproduction at high energies: From the Regge regime to the hard scattering regime. *Phys. Lett. B* **1997**, *400*, 6–11. [[CrossRef](#)]

20. Laget, J.M. Exclusive meson photo- and electro-production, a window on the structure of hadronic matter. *Prog. Part. Nucl. Phys.* **2020**, *111*, 103737. [[CrossRef](#)]
21. Laget, J.M. Unitarity constraints on meson electroproduction at backward angles. *Phys. Rev. C* **2021**, *104*, 025202.
22. Pire, B.; Semenov-Tian-Shansky, K.; Szymanowski, L. QCD description of backward vector meson hard electroproduction. *Phys. Rev. D* **2015**, *91*, 094006.
23. Chernyak, V.L.; Ogloblin, A.A.; Zhitnitsky, I.R. Calculation of exclusive processes with baryons. *Z. Phys. C* **1989**, *42*, 583–593. [[CrossRef](#)]
24. King, I.; Sachrajda, C.T. Nucleon wave functions and QCD sum rules. *Nucl. Phys. B* **1987**, *279*, 785–803. [[CrossRef](#)]
25. Li, W.B.; Huber, G.M.; Stevens, J.R.; Semenov-Tian-Shansky, K.; Szymanowski, L.; Pire, B.; Amarian, M.; Androic, D.; Aniol, K.; Armstrong, D.; et al. Backward-angle exclusive π_0 production above the resonance region. *arXiv* **2020**, arXiv:2008.10768. [[CrossRef](#)]
26. Lansberg, J.; Pire, B.; Semenov-Tian-Shansky, K.; Szymanowski, L. A consistent model for πN transition distribution amplitudes and backward pion electroproduction. *Phys. Rev. D* **2012**, *85*, 054021. [[CrossRef](#)]
27. Accardi, A.; Albacete, J.L.; Anselmino, M.; Armesto, N.; Aschenauer, E.C.; Bacchetta, A.; Boer, D.; Brooks, W.K.; Burton, T.; Chang, N.-B.; et al. Electron-Ion Collider: The next QCD frontier—Understanding the glue that binds us all. *Eur. Phys. J.* **2016**, *A52*, 268. [[CrossRef](#)]
28. Aschenauer, E.; Kiselev, A.; Petti, R.; Ullrich, T.; Horn, T.; Furltova, Y.; Nadel-Turowski, P.; Gonella, P.; Jones, P.; Ilieva, Y.; et al. *Electron-Ion Collider Detector Requirements and R&D Handbook*; Brookhaven National Laboratory: Upton, NY, USA, 2020. Available online: <http://www.eicug.org/web/> (accessed on 1 April 2020).
29. Abdul Khalek, R.; Accardi, A.; Adam, J.; Adamiak, D.; Akers, W.; Albaladejo, M.; Al-bataineh, A.; Alexeev, M.G.; Ameli, F.; Antonioli, P.; et al. Science requirements and detector concepts for the Electron-Ion Collider. EIC Yellow Report. *arXiv* **2021**, arXiv:2103.05419. [[CrossRef](#)]
30. Willeke, F.; Beebe-Wang, J. *Electron Ion Collider Conceptual Design Report 2021*; Brookhaven National Lab. (BNL): Upton, NY, USA; Thomas Jefferson National Accelerator Facility (TJNAF): Newport News, VA, USA, 2021. [[CrossRef](#)]
31. Hauenstein, F.; Jentsch, A.; Pybus, J.R.; Kiral, A.; Baker, M.D.; Furltova, Y.; Hen, O.; Higinbotham, D.W.; Hyde, C.; Morozov, V.; et al. Measuring recoiling nucleons from the nucleus with the Electron Ion Collider. *arXiv* **2021**, arXiv:2109.09509. [[CrossRef](#)]
32. Ryckebusch, J.; Debruyne, D.; Lava, P.; Janssen, S.; Van Overmeire, B.; Van Cauteren, T. Relativistic formulation of Glauber theory for $A(e, e\text{-prime } p)$ reactions. *Nucl. Phys. A* **2003**, *728*, 226–250. [[CrossRef](#)]
33. Martinez, M.C.; Lava, P.; Jachowicz, N.; Ryckebusch, J.; Vantournhout, K.; Udias, J.M. Relativistic models for quasi-elastic neutrino scattering. *Phys. Rev. C* **2006**, *73*, 024607.
34. Cosyn, W.; Martinez, M.C.; Ryckebusch, J. Color transparency and short-range correlations in exclusive pion photo- and electroproduction from nuclei. *Phys. Rev. C* **2008**, *77*, 034602.
35. Cosyn, W.; Ryckebusch, J. Nuclear ρ meson transparency in a relativistic Glauber model. *Phys. Rev. C* **2013**, *87*, 064608.
36. Farrar, G.R.; Liu, H.; Frankfurt, L.L.; Strikman, M.I. Transparency in nuclear quasiexclusive processes with large momentum transfer. *Phys. Rev. Lett.* **1988**, *61*, 686–689. [[CrossRef](#)] [[PubMed](#)]
37. Frankfurt, L.L.; Greenberg, W.R.; Miller, G.A.; Sargsian, M.M.; Strikman, M.I. Color transparency effects in electron deuteron interactions at intermediate Q^2 . *Z. Phys. A* **1995**, *352*, 97–113.
38. Carroll, A.S.; Barton, D.S.; Bunce, G.; Gushue, S.; Makdisi, Y.I.; Heppelmann, S.; Courant, H.; Fang, G.; Heller, K.J.; Marshak, M.L.; et al. Nuclear transparency to large angle pp elastic scattering. *Phys. Rev. Lett.* **1988**, *61*, 1698–1701. [[CrossRef](#)] [[PubMed](#)]
39. Brodsky, S.J.; de Teramond, G.F. Spin correlations, QCD color transparency and heavy quark thresholds in proton-proton scattering. *Phys. Rev. Lett.* **1988**, *60*, 1924–1927. [[CrossRef](#)] [[PubMed](#)]
40. Ralston, J.P.; Pire, B. Fluctuating proton size and oscillating nuclear transparency. *Phys. Rev. Lett.* **1988**, *61*, 1823–1826. [[CrossRef](#)] [[PubMed](#)]
41. Lee, T.S.H.; Miller, G.A. Color transparency and high-energy $(p, 2p)$ nuclear reactions. *Phys. Rev. C* **1992**, *45*, 1863–1870. [[CrossRef](#)]
42. Bhetuwal, D.; Matter, J.; Szumila-Vance, H.; Kabir, M.L.; Dutta, D.; Ent, R.; Abrams, D.; Ahmed, Z.; Aljawrneh, B.; Alsalmi, S.; et al. Ruling out color transparency in quasielastic $^{12}\text{C}(e, e'p)$ up to Q^2 of $14.2 (\text{GeV}/c)^2$. *Phys. Rev. Lett.* **2021**, *126*, 082301. [[CrossRef](#)]
43. Jain, P.; Pire, B.; Ralston, J.P. The status and future of color transparency and nuclear filtering. *arXiv* **2022**, arXiv:2203.02579. [[CrossRef](#)]
44. Pire, B.; Semenov-Tian-Shansky, K.M.; Shaikhutdinova, A.A.; Szymanowski, L. Backward timelike Compton scattering to decipher the photon content of the nucleon. *arXiv* **2022**, arXiv:2201.12853. [[CrossRef](#)]
45. Lansberg, J.; Pire, B.; Semenov-Tian-Shansky, K.; Szymanowski, L. Accessing baryon to meson transition distribution amplitudes in meson production in association with a high invariant mass lepton pair at GSI-FAIR with $\bar{\text{P}}\text{ANDA}$. *Phys. Rev. D* **2012**, *86*, 114033. Erratum in *Phys. Rev. D* **2013**, *87*, 059902. [[CrossRef](#)]
46. Pire, B.; Semenov-Tian-Shansky, K.; Szymanowski, L. Backward charmonium production in πN collisions. *Phys. Rev. D* **2017**, *95*, 034021. [[CrossRef](#)]